IEEE Access
Multidisciplinary | Rapid Review | Open Access Journal

Received November 24, 2021, accepted December 15, 2021, date of publication January 14, 2022, date of current version January 21, 2022.

Digital Object Identifier 10.1109/ACCESS.2022.3143164

Wideband Dual-Polarized 3D Printed Quad-Ridged Horn Antenna

FOLIN OKTAFIANI[1,2], (Member, IEEE), EFFRINA YANTI HAMID[1], (Member, IEEE), AND ACHMAD MUNIR[1], (Senior Member, IEEE)

[1]Radio Telecommunication and Microwave Laboratory, School of Electrical Engineering and Informatics, Institut Teknologi Bandung, Bandung 40132, Indonesia
[2]Research Center for Electronics and Telecommunication, National Research and Innovation Agency, Bandung 40135, Indonesia

Corresponding author: Achmad Munir (munir@ieee.org)

This work was supported in part by the National Research and Innovation Agency through the SAINTEK 2018 Project; in part by the Excellency Researches Scheme; and in part by the Researches, Community Services, and Innovation Program, Institut Teknologi Bandung, in 2022.

ABSTRACT This paper presents the development of a wideband dual-polarized 3D printed quad-ridged horn antenna (QRHA) that can be used for detecting and imaging applications. The QRHA consists of three main parts: the waveguide transducer, the horn, and the ridges. The waveguide transducer is modified into a square shape to obtain dual-polarization. Four variations of ridges were carried out to determine the ridge that best satisfies the required specifications, especially the bandwidth and sidelobe levels. Among the four ridge profiles, the quadratic model was used for the proposed QRHA as it generated the widest bandwidth and enhanced a lower operating frequency, which is beneficial for improving resolution and penetration depth. The double-ridged horn antenna (DRHA) was also investigated in order to make a comparison with QRHA's performance. The characterization results show that when compared to DRHA, QRHA performs better in terms of bandwidth, beamwidth, gain, and side lobe suppression. Due to the benefits it provides, 3D printing based on polylactic acid (PLA) material was selected as the manufacturing process for the proposed QRHA. The fabricated QRHA had a weight that was three times lighter compared to conventional antennas. The measurement results indicate that the 3D printed QRHA has the wideband characteristics of a –10 dB working bandwidth of 7.9 GHz in frequency ranges of 3.5 GHz to 11.4 GHz. Isolation between the ridges below –20 dB was achieved for most frequency ranges. Co– and cross-polarizations were also performed to evaluate the dual-polarization of the proposed QRHA. The radiation patterns showed that the measurement results agree well with the simulations for low, middle, and high operating frequencies.

INDEX TERMS Quad-ridged horn antenna, ridge profile, wideband, dual-polarization, PLA-based 3D printing.

I. INTRODUCTION

Quad-ridged horn antennas (QRHA) have been widely used in radio astronomy, electromagnetic compatibility (EMC) applications, microwave communications, radar systems, and in biomedical usage [1]. QRHA has shown promising potential in detecting and imaging applications due to its outstanding characteristics. Its wideband properties are beneficial for improving imaging quality and accuracy in object reconstruction [2]–[6]. Unidirectional patterns generated by QRHA are useful for transceiving signals with higher power for certain directions as well as decreasing unwanted signal interference from other directions, which means that QRHA is suitable for improving antenna performance [7]. A dual-polarization established by QRHA also allows the antenna to simultaneously radiate signals with horizontal and vertical polarizations, which is an important feature in tumor detection [8]. Research on QRHA as part of the detection process in biomedical engineering reveals that a dual-polarized antenna can improve sensitivity in detecting asymmetrical objects [9]. The performance of double-ridged horn antennas (DRHA), another type of ridged horn antenna, has been compared to those of QRHA. The results have substantiated that QRHA yields better performances compared to DRHA in terms of the reflection coefficient, radiation pattern, and gain [10].

The associate editor coordinating the review of this manuscript and approving it for publication was Qi Luo.

The most common method that is frequently implemented to manufacture QRHA is the computer numerical control (CNC) milling machine. This type of milling machine has numerous benefits: robustness, solid structure, along with durability and high density. The main advantage of the CNC milling machine is its high conductivity due to the metallic conductor material used. However, the complex structure of horn antennas requires precise dimensions which are difficult to achieve using the CNC milling method [11]–[12]. Some additional disadvantages include high costs and time-consuming manufacturing process. It is also heavy in weight due to being an all-metal construction [13]–[15]. On the other hand, an imaging application requires a lightweight antenna to facilitate portable detection processes. The process of object reconstruction in imaging application actually requires that QRHA be distributed over the entire object to achieve high detection sensitivity. As a result, low-cost fabrication techniques are needed since a great many QRHAs are required.

The invention of 3D printing makes it possible to overcome the limitations of manufacturing horn antennas using the CNC milling machine [16]. 3D printing has already attracted public attention due to its many advantages, such as producing precision dimensions, relatively low costs, and less time consuming to use. An outstanding characteristic of 3D printing is its capability to produce precise dimensions. It can also simplify the construction of antenna structures having small dimensions, tight gaps, and slight holes.

There are two types of 3D printers: metal-based and plastic-based. Metal-based 3D printing has similar benefits to those of the CNC milling machine, albeit even more precise in its dimensions. There is a large body of research regarding the production of horn antennas using metal-based 3D printing [16]–[20]. However, using metal-based 3D printing requires more time and additional processes, such as smoothing the horn antenna surface, in order to obtain a perfect end product. The limited availability of metal 3D printers and operators with the specific skills required to operate these printers also present additional drawbacks.

On the other hand, plastic-based 3D printing offers a simpler production process involving relatively less time and lower costs, as well as being lightweight and having a robust manufacturing process [21]–[23]. Moreover, the wide availability of this type of 3D printer and the fact that no special skills are needed to operate these machines give plastic-based 3D printers additional value. The filaments that are generally used in 3D printers are made of polylactic acid (PLA) and acrylonitrile butadiene styrene (ABS). PLA is the most often used due to having better properties, such as higher strength and stiffness, low melting temperature, no shrinkage, and simple to implement. PLA is also made from organic materials and supports environmental protection, while ABS is produced from petroleum-based materials. After making a comparison of the properties of both filaments, the PLA is most often selected for plastic-based 3D printing.

Utilization of PLA-based 3D printing to realize a horn antenna has been implemented in many research works, however most of these were concerned with the design of 3D printed horn antennas for single polarization [24]–[26]. Based on the aforementioned explanation, this paper aims to develop a PLA-based 3D printed QRHA that has a wide bandwidth and can accommodate the need for penetration depth and high resolution for imaging applications as well as generating dual-polarization. Bandwidth improvement at a lower operating frequency was achieved by varying QRHA ridge profiles. A 3D printing technology using PLA as a material was used to produce an antenna that is lightweight, low cost, precise dimensions, and simple fabrication.

The rest of this paper is organized as follows: In Section II, the design of QRHA is discussed. This section presents a performance comparison between QRHA and DRHA with variations of ridge profiles, and the characteristics of an antenna produced using 3D printing. The manufacturing process of the proposed QRHA using 3D printing is described in Section III, followed by characterizations and discussion of results in Section IV. The conclusion of paper is presented in Section V.

II. QUAD-RIDGED HORN ANTENNA DESIGN

A. QUAD-RIDGED HORN ANTENNA

Generally, the QRHA design has the same construction as conventional horn antennas: both consist of a waveguide transducer and horn. An additional factor that plays a role in the QRHA construction is the utilization of ridge profiles which are inserted at the midpoint of the horn. The design of QRHA will be presented in this paper as the continuation of work done in [27]. The proposed QRHA consists of a waveguide transducer which uses a rectangular waveguide of WR90. The WR90 rectangular waveguide is modified into a square shape with the square waveguide transducer having an inside dimension of 22.86 mm $\times$ 22.86 mm. This is carried out in order to construct a dual-polarized horn antenna. Theoretically, the horn will have a TE_{10} operating frequency of 8.5 GHz to 12.5 GHz with a cut-off frequency of 6.5 GHz. The dimensions of the horn are set to create a compact size with a length and aperture width of 50.00 mm and 45.72 mm, respectively. The ridge profile employed in the preliminary QRHA design utilizes a common ridge profile. In order to gain optimum performance, the space between ridges was set at 3.75 mm with a ridge thickness of 3.25 mm.

The excitation of both ports in the proposed QRHA, i.e., port #1 and port #2 was done using 50 Ω sub-miniature version A (SMA) connectors. The center pin of the connector extended into the waveguide transducer part and was attached to the upper ridge. The position of port #2 was shifted slightly back from port #1 to avoid intersection between the centre pins of the connector.

DRHA has also been discussed as part of a comparison of horn antennas with differing ridge profiles. The geometry of the width and length of the waveguide and horn of DRHA

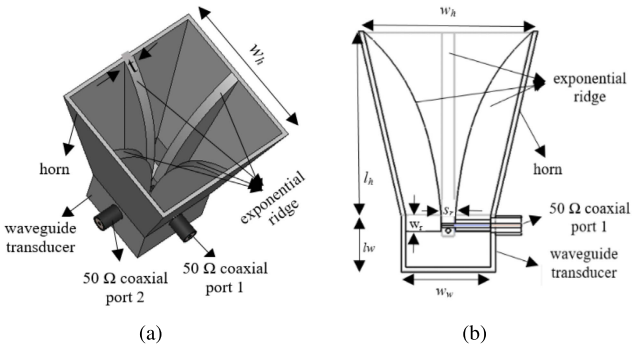

(a) (b)

FIGURE 1. Configuration of QRHA (a) perspective view, (b) cross-section view.

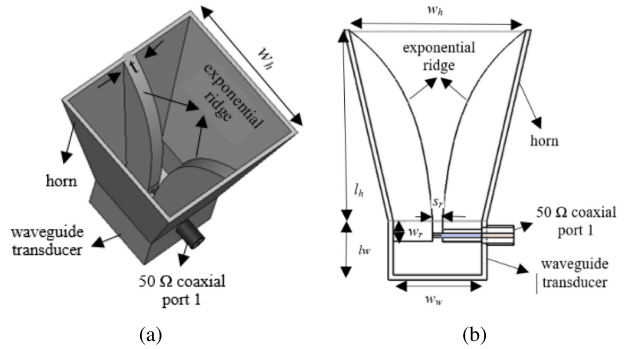

(a) (b)

FIGURE 2. Configuration of DRHA (a) perspective view, (b) cross-section view.

TABLE 1. Dimensions of QRHA and DRHA.

Parameter	Description	Dimension (mm)	
		QRHA	DRHA
w_w	width of waveguide part	22.86	22.86
l_w	length of waveguide part	14.00	14.00
w_h	width of horn part aperture	45.72	45.72
l_h	length of horn	50.00	50.00
t	thick of ridge	3.25	4.25
w_r	width of ridge	4.33	5.33
s_r	separation between ridges	3.75	2.50

has a similar configuration with the QRHA design; although some parameters of DRHA, such as ridge thickness, width of the ridges, and the separation between the ridges are set to have a slightly different dimension in order to achieve optimum performance. The DRHA ridges have a thicker dimension, and there is a closer space between the ridges when compared to QRHA, since there is no potential for the ridges to interact. The geometries of the proposed QRHA and DRHA constructed with 1.3 mm thick aluminium are depicted in Figs. 1 and 2, respectively, while details of the dimensions are summarized in Table 1.

B. VARIATIONS IN RIDGE PROFILES

The insertion of a ridge profile into part of the conventional horn antenna has the effect of decreasing the cut-off frequency. Therefore, the operating frequency range of

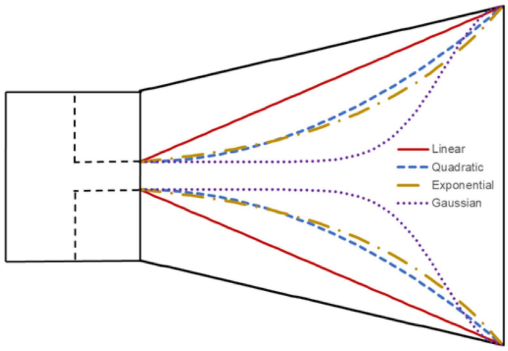

FIGURE 3. Four variations of ridge profile utilized into horn part.

the ridged horn antenna can be extended, compared to conventional horn antenna having similar dimensions which are not able to do so. The utilization of the ridges also contributes to the impedance matching between the feeding point at the waveguide transducer and the free space. The appropriate design of the ridge profile is a key factor in conducting impedance transition from the feeding point to the free space. An investigation of the different types of ridge profiles employed in DRHA was discussed in [28], while the influence of varying ridge profiles in QRHA was explored in [29], which will also be covered in this paper. Variations in ridge profiles were investigated to determine the most suitable profile which can give optimum performance. A similar investigation was also conducted for DRHA in order to compare the performances of both antennas.

The four ridge profiles investigated were: linear, quadratic, exponential and Gaussian, as illustrated in Fig. 3. The formulas for constructing the geometry of the ridge profiles for linear, quadratic, exponential, and Gaussian are given in (1) through (4), respectively. The geometry of the four ridge profiles has a different curve shape, which represents an impedance transition between the feed point and the free space. This shows that each ridge profile has an unequal impedance transition, which will generate a dissimilar response. The linear ridge profile produces the same impedance transition along the length of the horn, while the impedance transition of the Gaussian ridge profile begins just in the middle of the horn's length. The quadratic and exponential ridge profiles have a similar impedance transition pattern in the beginning. However, the exponential profile yields a wider curve shape at its ends than the quadratic.

$$y(z) = \left(\frac{w_h - s_r}{2l_h}\right)z + \frac{s_r}{2} \qquad 0 \le z \le l_h \tag{1}$$

$$y(z) = \left(\frac{w_h - s_r}{2l_h^2}\right)z^2 + \frac{s_r}{2} \qquad 0 \le z \le l_h \tag{2}$$

$$y(z) = \frac{s_r}{2}\exp\left[\frac{1}{l_h}\ln\left(\frac{w_h}{s_r}\right)z\right] \qquad 0 \le z \le l_h \tag{3}$$

$$y(z) = \exp\left[-4\pi\left(\frac{w_h - s_r}{2}\right)\left(\frac{z}{l_h - 10}\right)^2\right] + \frac{s_r}{2} \quad 0 \le z \le l_h \tag{4}$$

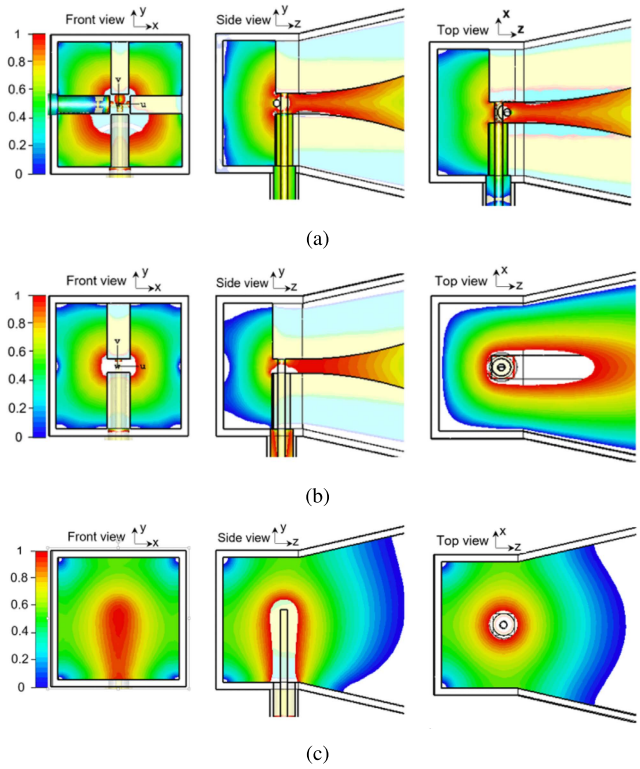

FIGURE 4. Normalized electric field distribution below the cut-off frequency of the conventional horn antenna on the (a) quad-ridged horn antenna, (b) double-ridged horn antenna, (c) conventional horn antenna.

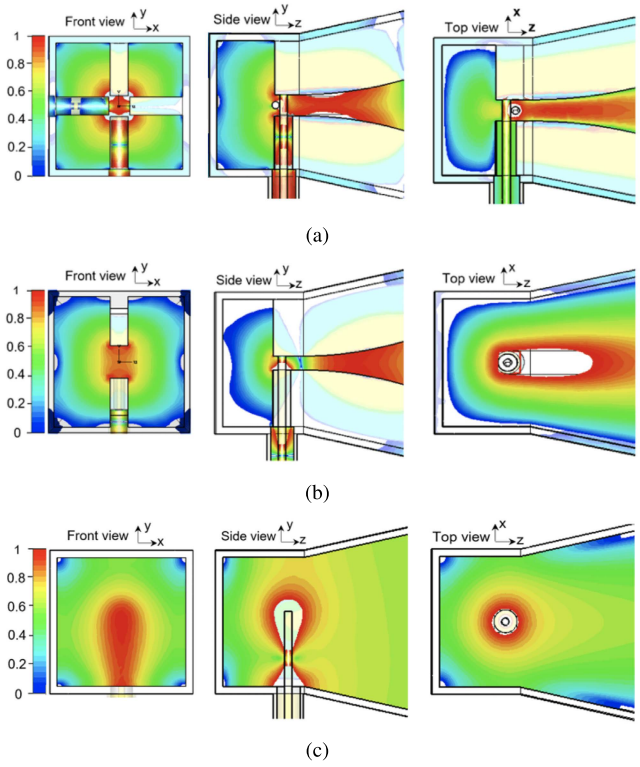

FIGURE 5. Normalized electric field distribution above the cut-off frequency of the conventional horn antenna on the (a) quad-ridged horn antenna, (b) double-ridged horn antenna, (c) conventional horn antenna.

Before comparing ridge profile variations between QRHA and DRHA, an investigation of the electric field distribution was carried out to determine the effect of additional ridge profiles on the operating frequency extension of the horn antenna. Three types of horn antennas, such as QRHA, DRHA and conventional horn antennas were demonstrated to inspect the electric field distribution. The quadratic profile was used as a profile ridge in the QRHA and DRHA designs. Observations were conducted at below and above cut-off frequencies of the conventional horn antenna, as depicted in Figs. 4 and 5, respectively. The electric field distribution of the QRHA, DRHA, and the conventional horn antenna and at front, side, and top views are presented to denote the electric field in detail. Based on the figures of normalized electric field distribution, there was no propagation of the electric field along the horn antenna for the conventional horn antenna at below cut-off frequency. The field starts to propagate at above frequencies, as seen in Figs. 4(c) and 5(c), while the QRHA and DRHA are capable of propagating electric fields even at below cut-off frequencies, as shown in Figs. 4(a) and 4(b). This reveals that the addition of ridge profiles is proven to decrease the cut-off frequency of horn antennas.

The side views of QRHA and DRHA indicate that the electric field of both antennas are still tightly confined in the gap regions, as depicted in Figs. 4(a) and 4(b). This condition also applies to QRHA on the horizontal side, as shown in the top view of Figs. 4(a) and 5(a). Based on these figures, it can be inferred that the ridged horn antenna has an advantage in that the electric field value can be maintained along with the presence of a ridge; furthermore, QRHA maintains an electrical field both vertically and horizontally. The intensity of the electrical fields of both QRHA and DRHA is stronger than conventional antennas because they have a narrower gap between their walls due to the presence of ridges.

The properties of QRHA and DRHA, including variations of ridge profiles, were then characterized using 3D simulation software to investigate the effect of ridge numbers and profiles. The results from the investigation can be considered as defining the number and the ridge profile that is most appropriate for the proposed design. Some antenna parameters were observed as evaluation performances for both horn antennas; these were: the reflection coefficient, radiation patterns, and gain. Additional observation was applied to the isolation between the ridges of QRHA. The characterization results for both QRHA and DRHA using four ridge profiles are depicted in Figs. 6–12.

From Figs. 6 and 7, it can be seen that four variations of ridge profiles generate almost the same bandwidth response for both horn antennas. Exponential ridge profiles produce a good reflection coefficient at high operating frequencies. Unfortunately, there is a deterioration in value for operating frequencies below 5 GHz.

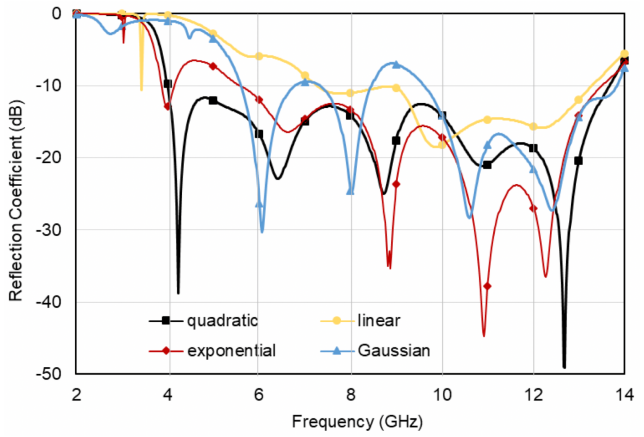

FIGURE 6. Characterization results of reflection coefficient for QRHA with varied ridge profiles.

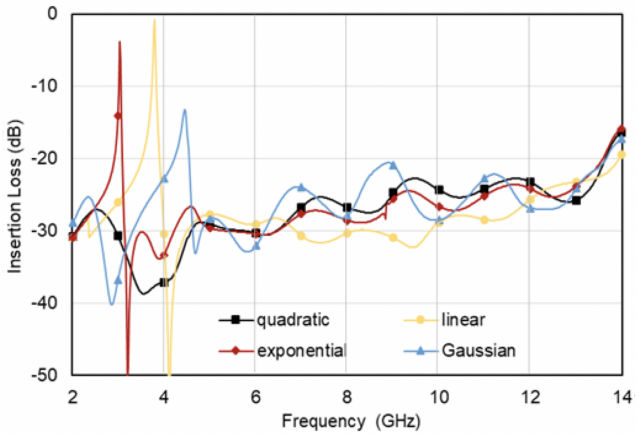

FIGURE 8. Characterization result of isolation between ports for QRHA with varied ridge profiles.

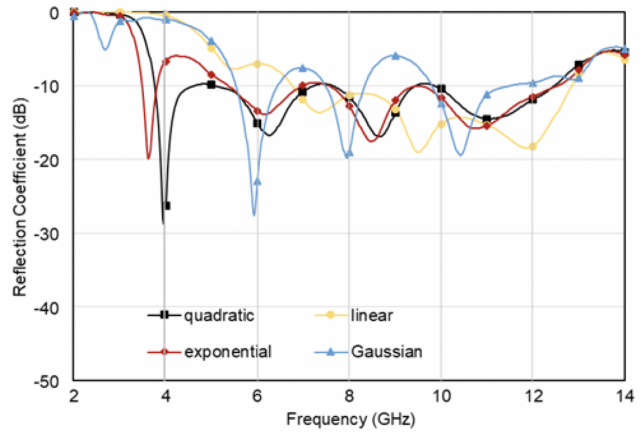

FIGURE 7. Characterization results of reflection coefficient for DRHA with varied ridge profiles.

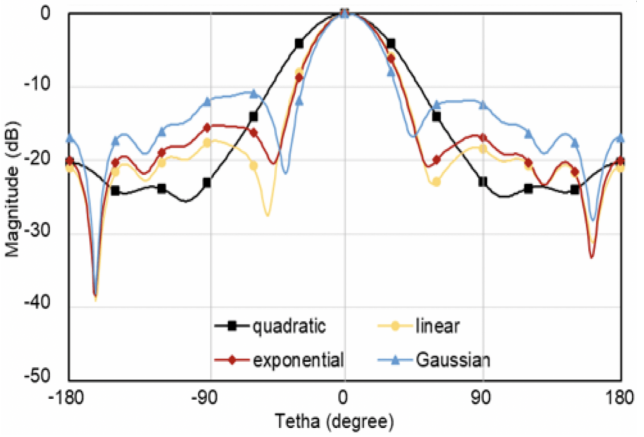

FIGURE 9. Characterization result of radiation pattern for QRHA with varied ridge profiles.

The quadratic ridge profile provides the widest impedance bandwidth for both horn antennas and offers better results, particularly in low frequencies with an impedance bandwidth for –10 dB reflection coefficient in frequency ranges from 4 GHz to 13 GHz. For a similar frequency range, the quadratic ridge profile also had a better isolation result between ports below –20dB, as shown in Fig. 8. The other ridges provided narrower impedance bandwidth and higher isolation between ports, especially at low operating frequencies. The characterization results of the reflection coefficient and the isolation between ports were also performed for port #2. These show that a slight difference occurs on port #2 for the reflection coefficient value due to shifting of the port positions. However, the reflection coefficient and isolation are in agreement with their accordance characteristics.

The observed radiation pattern of both QRHA and DRHA focus on an 8 GHz operating frequency. The radiation patterns for both antennas with different ridge profiles are shown in Figs. 9 and 10. There is no significant difference between the two horn antennas. The Gaussian ridge produced a narrower beamwidth, as can be seen in the figure aforementioned; nevertheless, the sidelobe level is unsatisfactory. On the other hand, the quadratic ridge has the lowest sidelobe level, below –20dB, although it generates the widest beamwidth for both horn antennas.

The gains for QRHA and DRHA are represented in Figs. 11 and 12, respectively. The highest gain for both antennas produced by the linear ridge profile paralleled the other ridge profiles in all operating frequencies between 8.5 GHz and 12.5 GHz. The quadratic and exponential ridge profiles have a similar tendency of gain for both QRHA and DRHA, while the quadratic ridge profile has a better gain than the other ones. The same holds true for the bandwidth response: the Gaussian ridge had the worst performance gain for both horn antennas.

The comparison results of both horn antennas for the observed parameters were applied in Table 2. Based on this table, it can be seen that QRHA produces a wider bandwidth of almost 1 GHz higher than DRHA. The better results of QRHA are also shown for antenna beamwidth; these show

TABLE 2. Results of comparison of quad-ridge and double-ridge horn antennas.

Parameter	QRHA				DRHA			
	Linear	Quadratic	Exponential	Gaussian	Linear	Quadratic	Exponential	Gaussian
Bandwidth (GHz)	6.17	9.69	8.10	4.29	6.14	8.76	7.40	2.27
Beamwidth (degree)	41.00	50.10	39.90	36.10	40.50	50.80	38.90	34.40
Maximum Gain (dBi)	15.58	13.51	13.19	10.90	14.93	13.02	11.98	10.57
Sidelobe Level (dB)	–17.70	–21.90	–15.40	–11.10	–17.80	–20.20	–15.00	–9.90
Isolation (dB)	< –22.00	< –20.00	< –20.00	< –20.00	-	-	-	-

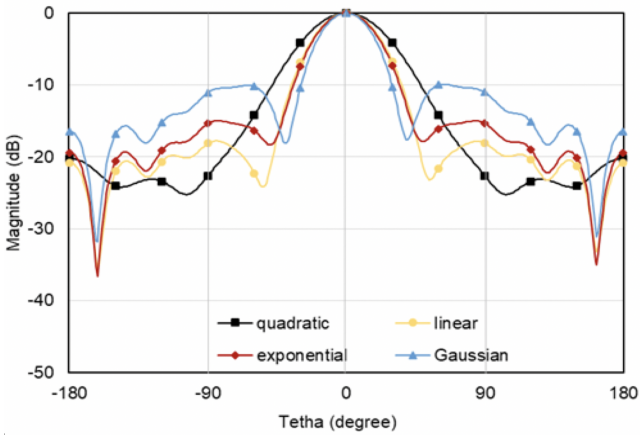

FIGURE 10. Characterization result of radiation pattern for DRHA with varied ridge profiles.

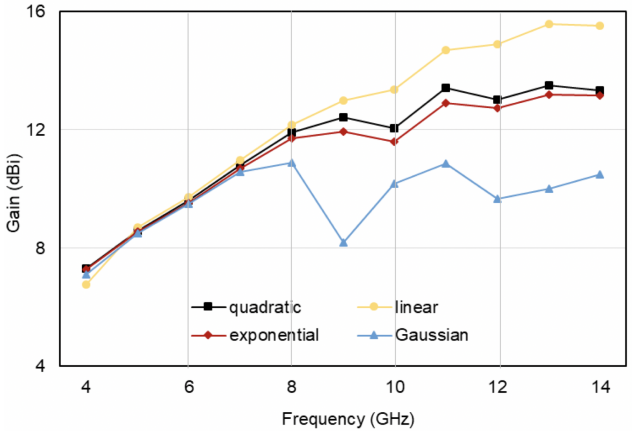

FIGURE 11. Characterization result of gain for QRHA with varied ridge profiles.

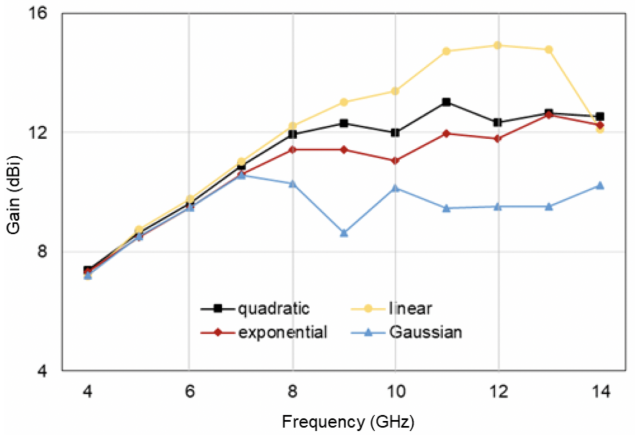

FIGURE 12. Characterization result of gain for DRHA with varied ridge profiles.

that QRHA obtained a narrower bandwidth than DRHA. Antenna gain as high as 0.5 dB was achieved by QRHA; therefore, it can be seen that implementing side lobe level parameters in QRHA results in better side lobe suppression. Based on these characterizations, it can be inferred that, when contrasted with DRHA, QRHA has better bandwidth, beamwidth, gain and sidelobe level characteristics.

Furthermore, concerning the performance characteristics of various ridge profiles for QRHA and DRHA, it can be seen that the quadratic ridge obtained the widest bandwidth for both antennas. In accordance with beamwidth, the Gaussian ridge profile obtained the narrowest beamwidth of all the ridges in both antennas. The highest gain was produced by using the linear ridge profile with QRHA and DRHA, followed by a quadratic ridge profile that had a slight difference in value. The variety of ridge profiles for QRHA and DRHA indicates that the quadratic ridge profile provides the lowest sidelobe level. From the prior explanation, it can be inferred that the quadratic ridge profile has a better performance for bandwidth and sidelobe levels when compared with the other profiles. Although the quadratic ridge profile has the widest beamwidth, the value is still tolerable. The proposed antenna can be useful in detecting and imaging applications; as a result, the focus of this research has been primarily on the bandwidth and sidelobe levels. Wide bandwidth is used to increase image reconstruction resolution, while a low sidelobe level is needed to prevent coupling between the antennas. By considering the performances of bandwidth, beamwidth, gain, and sidelobe level, it can be deduced that the quadratic ridge is the best ridge profile for horn antenna. Thus, we conclude that the best proposed horn antenna is the one that uses QRHA with a quadratic ridge profile.

C. PLA-BASED 3D PRINTED CHARACTERISTIC

3D printing is a new type of manufacturing technology that has recently come into widespread use. However, the characteristics of metal-based 3D printing yield a rough surface finish which will affect the propagation of electromagnetic waves [29]. In this section, the characteristics of PLA-based

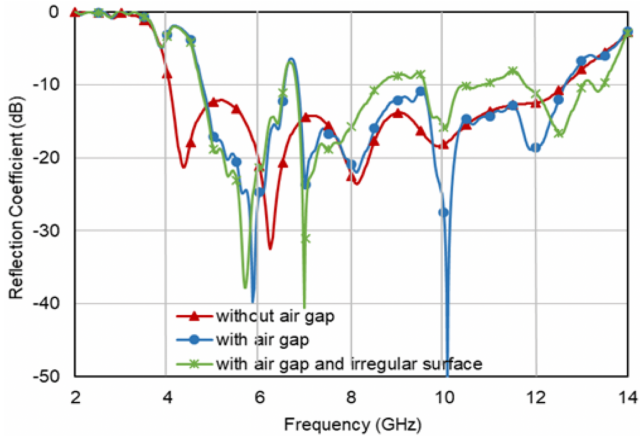

FIGURE 13. Effect of air gap and irregular surface to the reflection coefficient.

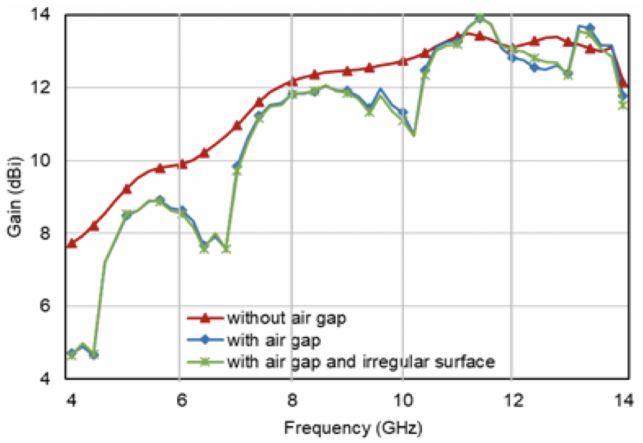

FIGURE 14. Effect of air gap and irregular surface to the antenna gain.

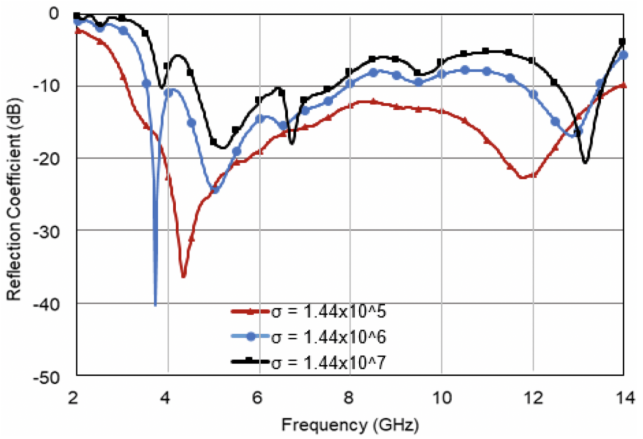

FIGURE 15. Effect of an impure conductivity to the reflection coefficient.

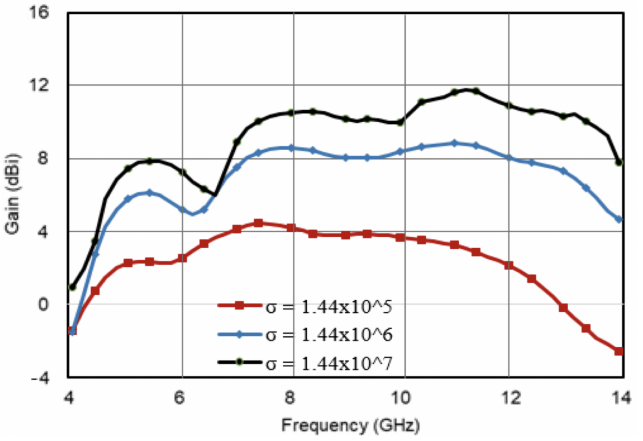

FIGURE 16. Effect of an impure conductivity to the antenna gain.

3D printing will be explored to find out its performance results, especially for bandwidth and gain. The fabrication technique of QRHA using PLA-based 3D printing requires a metallization process with impure conductive materials. In order to simplify these processes, the proposed QRHA antenna has been split into several parts. Surface smoothness and irregular thickness in the inside of the horn antenna and ridge profile are some issues that are unavoidable in the metallization process. There is also an air gap between parts of the horn antenna which is unpreventable as it is due to the process of integrating all of the parts. The impure conductivity value of the coating material will also impact the directivity and gain of the proposed horn antenna. In considering the effectiveness of using 3D printing, it is necessary to investigate the results of impure conductivity and imperfect fabrication on the performance of horn antennas in terms of operating frequency and gain. These effects include air gaps, as well as the irregular thickness of the inside and ridge surfaces.

The consequences of splitting QRHA into several parts means that the geometry of the antenna cannot be closely combined, which results in an air gap between the parts. The effect of air gaps on QRHA performance still needs to be investigated; particularly for such antenna parameters as the reflection coefficient and antenna gain. Alterations in the reflection coefficient and antenna gain characteristics of QRHA that result from air gaps are shown in Figs. 13 and 14. From Fig. 13, it can be seen that an air gap alters the operating frequency and decreases the horn antenna bandwidth as depicted by a blue line. A similar response also occurs in antenna gain which has decreased values with the presence of air gaps, as shown in Fig. 14.

The imperfect fabrication and metallization process is responsible for the roughness of the QRHA inside surface, which, in turn, influences the reflection coefficient and gain antenna. An investigation of the imperfect fabrication and metallization is illustrated in Figs. 13 and 14. A characterization of the designed QRHA with added air gaps was also carried out, as seen in Fig. 13. The figure shows a narrower antenna bandwidth, as represented in Fig. 13 by a green line. At the same time, the antenna gain with a surface roughness had the same response as when air gaps were present, as shown in Fig. 14.

The metallization process uses ink that contain metal. The metal ink that is available commercially is a mixture of materials that results in a product with impure and unknown conductivity value. Since the antenna is coated with this impure conductivity material, it will affect the antenna radiation characteristics, particularly antenna gain. A simulation of QRHA using an ink that has impure conductivity was carried out in order to evaluate the effect of metallic levels on the reduction of antenna gain. The percentages of metallic level of a material was indicated based on its conductivity value, although these percentage cannot be represented linearly in the conductivity value. Therefore, the characterization of impure conductivity was performed by varying the conductivity values of the coating material. The conductivity was variated by using three grades of conductivity value where the value degrades ten times the actual value of the material's conductivity, these were: 1.44×10^7 S/m, 1.44×10^6 S/m, 1.44×10^5 S/m. We investigated the effect of the antenna coated with an impure conductivity material on the reflection coefficient and antenna gain of the proposed QRHA; the results are illustrated in Figs. 15 and 16. The reduction of antenna gain is in line with the conductivity value, which indicates that lower metallic content will yield lower gain antenna.

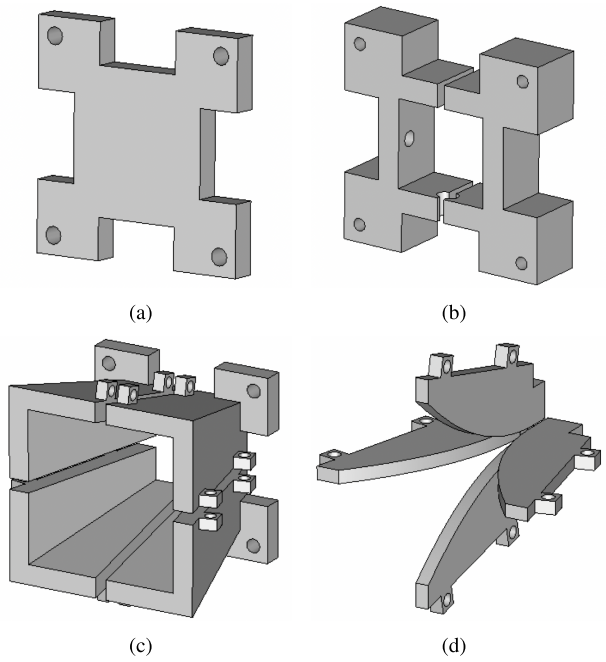

FIGURE 17. Parts of proposed 3D printed QRHA: (a) waveguide back cover, (b) waveguide side walls, (c) horn antenna section, (d) quadratic ridged profile.

III. MANUFACTURING OF 3D-PRINTED QRHA

The method that is most commonly used to manufacture horn antennas is CNC milling. Unfortunately, this method has drawbacks, especially in terms of being time-consuming and costly and also involves a complex manufacturing process. 3D printing is a fairly new method that is catching the attention of many researchers because it is able to achieve precise dimensions in simulation designs, particularly for complicated structures. Considering that the arch shape of the ridge profile needs to be constructed precisely, 3D printing was selected as the best way to manufacture QRHA in this research.

Utilization of 3D printing makes it feasible to generate QRHA as a single part; however, the material used to print the proposed antenna is non-metallic so a coating process is needed. As a result, the proposed design antenna was divided into several parts to simplify the prototyping and metallization process after which the parts would be reintegrated and assembled, using bolts and nuts. The individual parts consist of the waveguide back cover, the waveguide sidewall, the horn section, and the quadratic ridge profile, as shown in Fig. 17. The thickness of the QRHA is set to 5 mm in order to provide space for installing a bolt in the SMA connector. This is intended to maintain the smoothness of the inside surface of the waveguide. The outside structure of the QRHA was modified to facilitate the process of re-integrating all the parts precisely. The configuration of the geometry of the outer surfaces of QRHA is undertaken in such a way that it does not affect the performance of the antenna.

There are three steps involved in fabricating the proposed QRHA: 3D printing, metallization, and assembling. The Raise 3D Pro2 Plus printer was used to perform the 3D printing process with PLA as the main material. The benefit of using this method is that it presents a simple process by which the designed antenna can be imported into the printing machine in order to obtain the prototype as required. This process also offers a low-cost fabrication process for the proposed QRHA with the possibility of doing mass production. The quadratic ridge profile with a precise curve shape is also easily realized using this technique. The next step is metallizing the surface of all the printed parts with a conductive material that uses nickel as a row material (Noise Hell SP-D-02 LACQUER^{TM}). After the metallization process, all the parts of the proposed QRHA are assembled. The assembly process is crucial because it determines whether the resulting antenna will be produced in the same size as the design. It is important to ensure that there is no misalignment when the parts are assembled and that all the parts connected properly without air gaps between them. Realizations of the proposed 3D printed QRHA before and after the metallization process are presented in Figs. 18 and 19, respectively. The total weight of the prototype 3D printed QRHA is around 300g, which is very light compared to conventional fabrication methods. 3D printing can produce a product that has a total weight three times lighter than those made using the CNC method.

IV. CHARACTERIZATIONS AND DISCUSSION

The measurements were experimentally implemented after the prototype was assembled correctly and installed to the SMA connector in order to compare these with the simulation results. The characterized experimental parameters were:

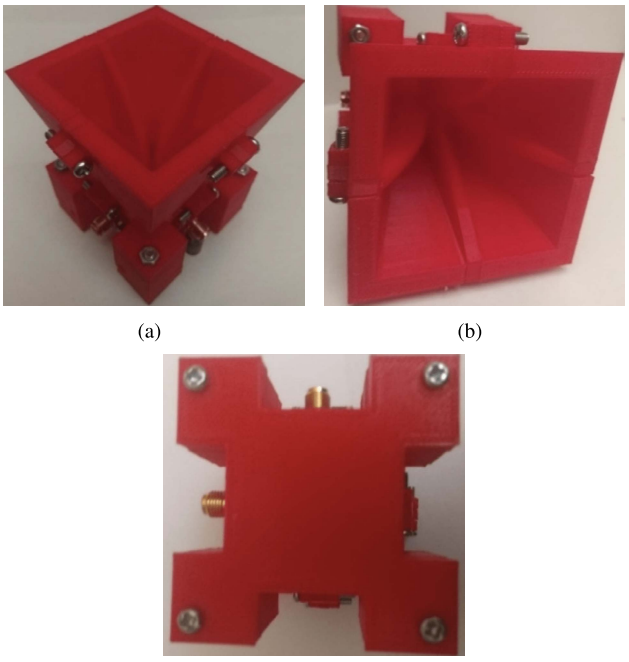

(a) (b) (c)

FIGURE 18. Realized 3D printed QRHA before metal coating process (a) perspective view, (b) front view, (c) back view.

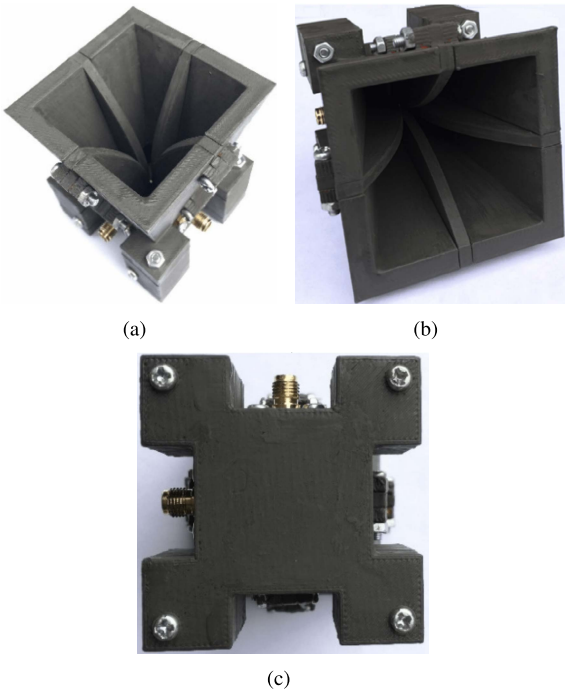

(a) (b) (c)

FIGURE 19. Realized 3D printed QRHA after metal coating process (a) perspective view, (b) front view, (c) back view.

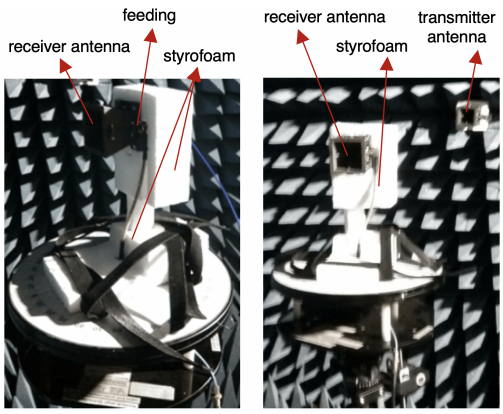

FIGURE 20. Measurement set up of 3D printed QRHA.

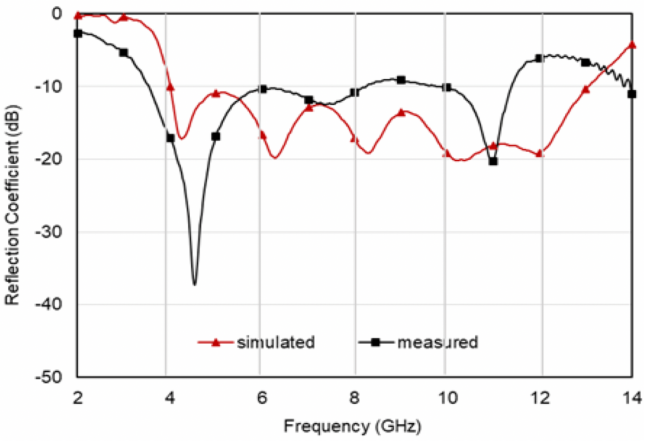

FIGURE 21. Comparison results of reflection coefficient between simulation and measurement.

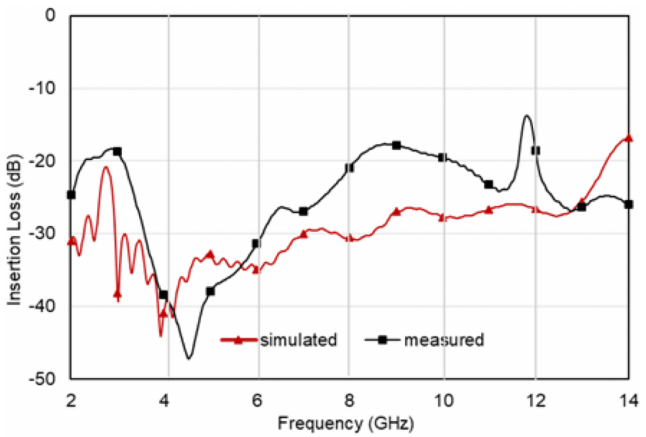

FIGURE 22. Comparison results of isolation between simulation and measurement.

the reflection coefficient, the isolation between ports, the radiation pattern, and antenna gain. In order to acquire the optimum results, the measurement of the radiation pattern and gain was carried out in an anechoic chamber of the university laboratory with the measurement set-up as depicted in Fig. 20. The measurement of gain and of the radiation pattern used two identical proposed 3D printed QRHAs with a distance of 1 m. The proposed antenna was installed with a holder made from styrofoam in order to make a space between the measurement boards. The purpose for this was

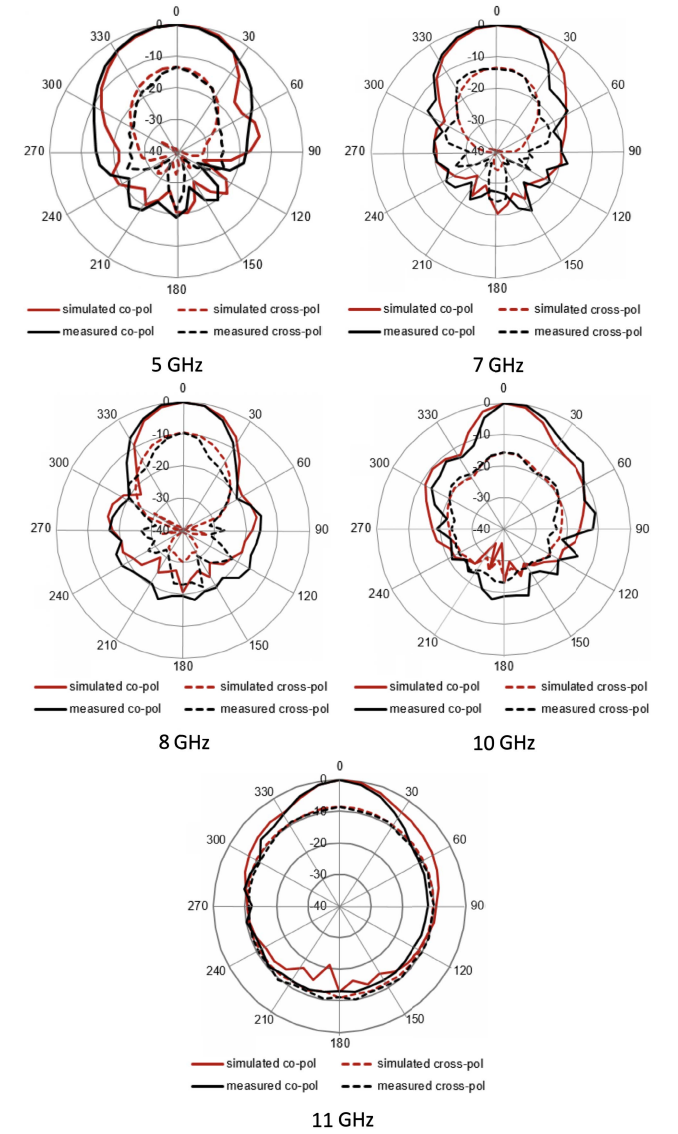

FIGURE 23. Co– and cross-polarization normalized radiation pattern of elevation angle.

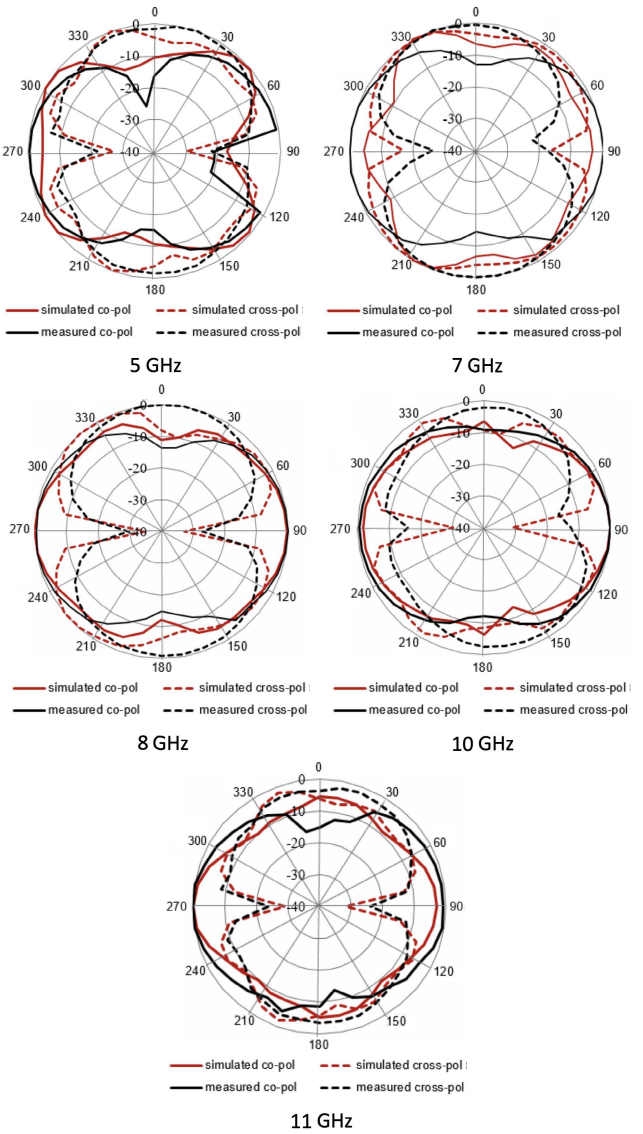

FIGURE 24. Co– and cross-polarization normalized radiation pattern of azimuth angle.

to minimize reflection from the measurement board so that it did not affect the antenna radiation pattern.

The characterization results of 3D printed QRHA, illustrated in Figs. 21–25, are for the reflection coefficient, the isolation between ports, the radiation pattern, and gain which were compared with the simulation results. Fig. 21 shows that the proposed 3D printed QRHA has an impedance bandwidth of –10 dB measured in the frequency range of 3.5–11.4 GHz. Compared to the simulated results, the result obtained is narrower by about 1 GHz, which had an impedance bandwidth in the frequency range of 4–13 GHz. The narrower measured operating bandwidth resulted because of the smoothness of the surface and the irregular thickness on the ridge profile as was characterized in Section IIC.

The presence of an air gap between the parts that cannot be avoided in the assembling process is also one of the factors that leads to different results between the simulation and the measurement. Another factor that induces a different response from the proposed fabricated antenna is the requirement for a long SMA inner connector that is unavailable in local markets. Instead, the inner connector was extended by connecting it the other inner using solder, which influences the impedance value of the connector. In addition, shifts in the operational frequency occurred in the measurement results, which were probably caused by the difference in thickness which could not be avoided during the metallization procedure, particularly in the inside surface part. As a result, the dimension alterations of QRHA were affected. However, based on the measurement results, the fabricated 3D printed QRHA generated a good performance in terms of the reflection coefficient and met with the required specifications for ultra-wide band characteristics.

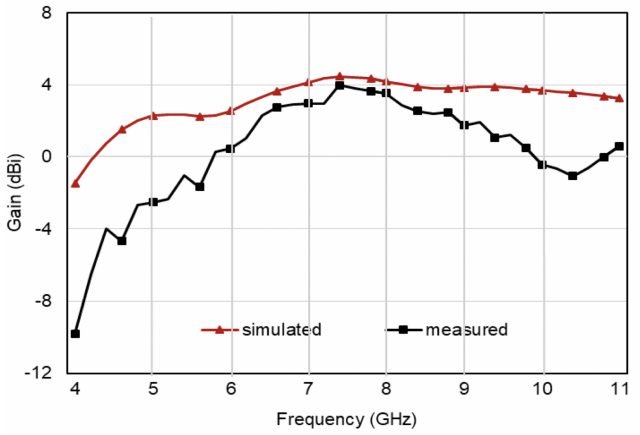

FIGURE 25. Comparison results of antenna gain between simulation and measurement.

Furthermore, isolation between the ports, as depicted in Fig. 22, shows that the fabricated 3D printed QRHA has qualitatively the same pattern, although the value of the transmission coefficient that was measured increased in frequency ranges higher than 6 GHz. Moreover, the isolation between the ports was more than 20 dB for the section of the operating frequency that could be reach by the proposed 3D printed QRHA. From the characterization results, it is inferred that the proposed 3D printed QRHA can be utilized in applications which require a wide bandwidth and high isolation in order to obtain object detection with a high resolution and deep penetration.

The next characterization of the 3D printed QRHA compared the measured radiation pattern of the fabricated antenna with one that was simulated. Observation of the radiation pattern was done in low, middle and high frequency covers; namely, 5 GHz, 7 GHz, 8 GHz, 10 GHz and 11 GHz. The measurement of co– and cross-polarization was performed by altering the excitation port in order to prove the capability of the dual-polarization feature. The radiation pattern of the proposed antenna was carried out in both elevation and azimuth angles. The measurement results of the normalized radiation patterns are described in Figs. 23 and 24. Fig. 23 denotes the results of the co– and cross-elevation radiation patterns, while the co– and cross-azimuth radiation patterns are shown in Fig. 24.

The results depicted in Fig. 23 reveal that the measured co-polarization normalized pattern for the elevation angle has a similar trend with the simulated one, although there were some different values for several angles. Similar to a cross-polarization normalized pattern, there were some discrepancies in the measured with the simulated result, particularly in low and middle frequencies. In fact, the elevation cross-polarization for 5 GHz had an almost identical pattern; there was a difference in the power received level, starting at an angle of 90 degrees. A similar response was also demonstrated for frequencies of 7 GHz and 8 GHz. This is because of the limited observation angle used in the measurement process. The power received was investigated towards an alteration position of 10 degrees due to the limitations of the supporting device. Another possible error was the misalignment of the position of the transmitter and receiver antennas because these were arranged manually. In addition, data retrieval of the power received was performed by observing the spectrum analyzer which generates fluctuations in value, so there was a possibility of inaccuracy in reading the measurement data.

Similar to the elevation angle, the measured normalized radiation pattern for the azimuth angle was seen as being the same as the simulation result, although there was a small difference on a particular frequency, as illustrated in Fig. 24. The difference between the simulated and measured radiation patterns clearly looks for co-polarization of 7 GHz; however, the characterizations of the other frequencies are in accordance with the simulated ones. Based on the measured radiation pattern, the elevation and azimuth angle for co– and cross-polarization for various frequencies show that the proposed antenna yields a good performance for dual-polarization applications.

Fig. 25 shows the measurement of the antenna gain of the proposed PLA-based 3D printed QRHA compared to the simulation results. The simulation results used to compare with the QRHA had a conductivity of 1.44×10^5 S/m. The proposed QRHA produced an antenna gain lower than that of the simulation for low-operating frequencies. This can be explained by referring to the characterization results described in Section IIC, Fig. 14 which explains that the decrease of antenna gain is due to air gaps and surface roughness. The antenna produces a low gain due to the lossy nickel conductive material and the impurity of the nickel particles. Based on the simulation, it can be inferred that the conductive material of the proposed QRHA contained only 20–40% nickel. Because the antenna is used for detecting and imaging systems in near range, a low gain antenna can still be applied to the system.

V. CONCLUSION

The wideband dual-polarized 3D printed QRHA based on PLA materials has been presented and experimentally characterized. The realized 3D printed QRHA generates a wide bandwidth and dual-polarization after the insertion of four ridges with a quadratic profile into the horn parts, thus meeting the requirements for detecting and imaging applications. A lightweight QRHA with compact and precise dimensions can be achieved by utilizing 3D printing. The characterizations of 3D printing show that imperfect fabrication conditions, such as air gaps and irregular thickness, increase the reflection coefficient value and results in reducing the antenna bandwidth. Since the amount of conductive materials (metal) in the antenna was only between 20% and 40%, the gain generated is low. It has been shown that the realized QRHA provides adequate performances in terms of the reflection coefficient, the isolation between ports, and the radiation pattern. The measurement results are also in

good agreement with those of the simulation, proving that 3D printing is a promising option in fabricating horn antennas.

REFERENCES

[1] A. Rojatkar and S. Ananthakrishnan, "Quad-ridge horn antenna analysis and design for radio astronomy applications," in *Proc. Indian Antenna Week (IAW)*, Dec. 2011, pp. 1–4, doi: 10.1109/IndianAW.2011.6264907.

[2] L. Riaz, "Design of ultra wideband antenna array for microwave tomography," M.S. thesis, Dept. Technol. Built Environ., Univ. Glave, Stockholm, Sweden, 2011.

[3] S. Gerritsen, "Waves in inhomogeneous media," Ph.D. dissertation, Kavli Inst. Nanosci., Tech. Univ. Delft, The Netherlands, 2007.

[4] Q. Fang, P. M. Meaney, and K. D. Paulsen, "Microwave image reconstruction of tissue property dispersion characteristics utilizing multiple-frequency information," *IEEE Trans. Microw. Theory Techn.*, vol. 52, no. 8, pp. 1866–1875, Aug. 2004, doi: 10.1109/TMTT.2004.832014.

[5] C. Gilmore, P. Mojabi, A. Zakaria, M. Ostadrahimi, C. Kaye, S. Noghanian, L. Shafai, S. Pistorius, and J. LoVetri, "A wideband microwave tomography system with a novel frequency selection procedure," *IEEE Trans. Biomed. Eng.*, vol. 57, no. 4, pp. 894–904, Apr. 2010, doi: 10.1109/TBME.2009.2036372.

[6] M. A. Al-Joumayly, S. M. Aguilar, N. Behdad, and S. C. Hagness, "Dual-band miniaturized patch antennas for microwave breast imaging," *IEEE Antennas Wireless Propag. Lett.*, vol. 9, no. 3, pp. 268–271, Mar. 2010, doi: 10.1109/LAWP.2010.2045871.

[7] N. Khalid, S. Z. Ibrahim, and M. N. A. Karim, "Directional and wideband antenna for ground penetrating radar (GPR) applications," in *Proc. 3rd Int. Conf. Electron. Design (ICED)*, Aug. 2016, pp. 203–206, doi: 10.1109/ICED.2016.7804637.

[8] D. T. Al-Zuhairi, J. M. Gahl, and N. E. Islam, "Compact dual-polarized quad-ridged UWB horn antenna design for breast imaging," *Prog. Electromagn. Res. C*, vol. 72, pp. 133–140, 2017, doi: 10.2528/PIERC16121405.

[9] H. Amjadi, F. T. Hamedani, and M. I. Zaman, "A comparison of double-ridged and quad-ridged horn antenna for microwave tumor detection," in *Proc. 15 Int. Symp. Antenna Technol. Appl. Electromagn.*, Jun. 2012, pp. 1–4, doi: 10.1109/ANTEM.2012.6262423.

[10] F. Oktafiani, E. Y. Hamid, and A. Munir, "Performance evaluation of quad-ridged horn antenna in variation of its ridge profile," in *Proc. TENCON IEEE Region Conf. (TENCON)*, Oct. 2019, pp. 214–217, doi: 10.1109/TENCON.2019.8929577.

[11] I. Gibson, D. Rosen, and B. Stucker, *Additive Manufacturing Technologies: Rapid Prototyping to Direct Digital Manufacturing*. Boston, MA, USA: Springer, 2010, doi: 10.1007/978-1-4419-1120-9.

[12] A. Genc, I. B. Basyigit, T. Goksu, and S. Helhel, "Investigation of the performances of X–Ku band 3D printing pyramidal horn antennas coated with the different metals," in *Proc. 10th Int. Conf. Electr. Electron. Eng. (ELECO)*, Bursa, Turkey, Dec. 2017, pp. 1012–1016.

[13] T.-W. Chiou, "Quad-ridged horn antenna with L shaped-slot fed by microstrip line," in *Proc. Int. Symp. Antennas Propag. Conf.*, Dec. 2014, pp. 243–244, doi: 10.1109/ISANP.2014.7026621.

[14] B. Majumdar, D. Baer, S. Chakraborty, K. P. Esselle, and M. Heimlich, "A 3D printed dual-ridged horn antenna," in *Proc. Int. Conf. Electromagn. Adv. Appl. (ICEAA)*, Sep. 2016, pp. 836–839, doi: 10.1109/ICEAA.2016.7731529.

[15] M. A. Al-Tarifi and D. S. Filipovic, "On the design and fabrication of W-band stabilised-pattern dual-polarised horn antennas with DMLS and CNC," *Microw., Antennas Propag.*, vol. 11, no. 14, pp. 1930–1935, Nov. 2017, doi: 10.1049/iet-map.2017.0167.

[16] J. C. S. Chieh, B. Dick, S. Loui, and J. D. Rockway, "Development of a Ku-band corrugated conical horn using 3-D print technology," *IEEE Antennas Wireless Propag. Lett.*, vol. 13, pp. 201–204, Feb. 2014, doi: 10.1109/LAWP.2014.2301169.

[17] Y. C. Toy, P. Mahouti, F. Gunes, and M. A. Belen, "Design and manufactering of an X-band horn antenna using 3-D printing technology," in *Proc. 8th Int. Conf. Recent Adv. Space Technol. (RAST)*, Jun. 2017, pp. 195–198, doi: 10.1109/RAST.2017.8002988.

[18] T. Chio, G. Huang, S. Zhou, and W. Lim, "A 3D-printed compact dual-circularly polarized corrugated horn with integrated septum polarizer," in *Proc. Int. Symp. Antennas Propag. (ISAP)*, Okinawa, Japan, Oct. 2016, pp. 272–273.

[19] A. Vosoogh, P. Kildal, V. Vassilev, A. U. Zaman, and S. Carlsson, "E-band 3-D metal printed wideband planar horn array antenna," in *Proc. Int. Symp. Antennas Propag. (ISAP)*, Okinawa, Japan, Oct. 2016, pp. 304–305.

[20] K. Kotze and J. Gilmore, "SLM 3D-printed horn antenna for satellite communications at X-band," in *Proc. IEEE-APS Topical Conf. Antennas Propag. Wireless Commun. (APWC)*, Sep. 2019, pp. 148–153, doi: 10.1109/APWC.2019.8870367.

[21] B. Zhang, L. Wu, Y. Zhou, Y. Yang, H. Zhu, and Y. Wu, "A 3D printed aluminum alloy K-band square stepped doubled ridged horn antenna," in *Proc. IEEE Int. Conf. Comput. Electromagn. (ICCEM)*, Mar. 2018, pp. 1–2, doi: 10.1109/COMPEM.2018.8496551.

[22] A. H. Wahyudi, J. T. Sri Sumantyo, A. S. Budiyanta, and A. Munir, "3D printed wideband circularly polarized pyramidal horn antenna," in *Proc. Prog. Electromagn. Res. Symp. (PIERS-Toyama)*, Aug. 2018, pp. 868–871, doi: 10.23919/PIERS.2018.8597894.

[23] A. H. Wahyudi, J. T. S. Sumantyo, S. Wijaya, and A. Munir, "PLA-based 3D printed circularly polarized X-band horn array antenna for CP-SAR sensor," in *Proc. Int. Workshop Antenna Technol. (iWAT)*, Mar. 2018, pp. 1–4, doi: 10.1109/IWAT.2018.8379219.

[24] R. A. Syafrindo, J. T. S. Sumantyo, C. E. Santosa, and A. Munir, "3D print X-band horn antenna for ground-based SAR application," in *Proc. Prog. Electromagn. Res. Symp. Spring (PIERS)*, May 2017, pp. 1250–1253, doi: 10.1109/PIERS.2017.8261940.

[25] S. Rashid, L. Jofre, A. Garrido, G. Gonzalez, Y. Ding, A. Aguasca, J. O'Callaghan, and J. Romeu, "3-D printed UWB microwave bodyscope for biomedical measurements," *IEEE Antennas Wireless Propaga. Lett.*, vol. 18, no. 4, pp. 626–630, Apr. 2019, doi: 10.1109/LAWP.2019.2899591.

[26] A. Molaei, A. Bisulco, L. Tirado, A. Zhu, D. Cachay, A. G. Dagheyan, and J. M-Lorenzo, "3-D-printed E-band compressive horn antenna for high-sensing-capacity imaging applications," in *Proc. IEEE Antennas Wireless Propag. Lett.*, vol. 17, no. 9, pp. 1639–1642, Sep. 2018, doi: 10.1109/LAWP.2018.2859912.

[27] F. Oktafiani, E. Y. Hamid, and A. Munir, "PLA-based 3D printed quad-ridged horn antenna for tomography application," in *Proc. Photon. Electromagn. Res. Symp. Fall (PIERS–Fall)*, Dec. 2019, pp. 1275–1279, doi: 10.1109/PIERS-Fall48861.2019.9021386.

[28] A. Genc, I. B. Basyigit, T. Goksu, and S. Helhel, "The comparison of the characteristics of the double-ridged horn antennas depending the geometry of ridge profiles for wideband application," in *Proc. Prog. Electromagn. Res. Symp. Spring (PIERS)*, May 2017, pp. 1553–1557, doi: 10.1109/PIERS.2017.8261994.

[29] C. R. Garcia, R. C. Rumpf, H. H. Tsang, and J. H. Barton, "Effects of extreme surface roughness on 3D printed horn antenna," *Electron. Lett.*, vol. 49, no. 12, pp. 734–736, Jun. 2013, doi: 10.1049/el.2013.1528.

FOLIN OKTAFIANI (Member, IEEE) received the B.E. degree in electrical engineering from the Universitas Gadjah Mada, Indonesia, in 2004, and the M.E. degree in telecommunication engineering from the School of Electrical Engineering and Informatics, Institut Teknologi Bandung, Indonesia, in 2011, where she is currently pursuing the Ph.D. degree in electrical engineering and informatics.

Since 2005, she has been working as a Research Associate with the Research Center for Electronics and Telecommunication, Indonesian Institute of Sciences (currently becoming the National Research and Innovation Agency). Her research interests include antenna design and microwave devices. She was a recipient of the Best Presenter Award and the Best Poster Presentation Award at the International Conference on Radar, Antennas, Microwave, Electronic, and Telecommunication (ICRAMET) in 2012 and 2017, respectively.

EFFRINA YANTI HAMID (Member, IEEE) was born in Indonesia, in 1972. She received the B.E. and M.E. degrees in electrical engineering from the Institut Teknologi Bandung, Indonesia, in 1995 and 1998, respectively, and the D.E. degree from the Department of Electrical Engineering, Osaka University, Japan, in 2002.

Since 1997, she has been a Lecturer with the Department of Electrical Engineering, Institut Teknologi Bandung. Since 2007, she has been an Assistant Professor with the School of Electrical Engineering and Informatics, Institut Teknologi Bandung, where she is currently the Head of the Telecommunication Engineering Study Program, School of Electrical Engineering and Informatics. Her main research interest includes the application of analog and digital signal processing for communication systems.

ACHMAD MUNIR (Senior Member, IEEE) received the B.E. degree in electrical engineering from the Institut Teknologi Bandung, Indonesia, in 1995, and the M.E. and D.E. degrees in science and engineering from Yamaguchi University, Japan, in 2002 and 2005, respectively.

From 2005 to 2007, he was a Research Fellow under JSPS Fellowship Program with the Faculty of Engineering, Yamaguchi University, working on the artificial materials research, particularly, artificial dielectric and artificial magnetic materials. From 2007 to 2009, he was a Research Fellow with the Institute of Electronics, Communication and Information Technology, Queens University Belfast, Northern Ireland, U.K., involved in the experimental study of novel nonlinear artificial material, including high-impedance surface and artificial magnetic conductor for advanced EM applications. In 2009, he joined the School of Electrical Engineering and Informatics, Institut Teknologi Bandung, where he is currently an Associate Professor. His research interests include linear and nonlinear artificial materials, electromagnetics wave propagation, and microwave and RF devices. He is the Editor-in-Chief of the *Journal of ICT Research and Applications*.